



# Time Reversed Absorbing Condition: Application to inverse problems

Franck Assous, Marie Kray, Frédéric Nataf, Eli Turkel

## ► To cite this version:

Franck Assous, Marie Kray, Frédéric Nataf, Eli Turkel. Time Reversed Absorbing Condition: Application to inverse problems. 2011. hal-00491912v2

**HAL Id: hal-00491912**

**<https://hal.science/hal-00491912v2>**

Preprint submitted on 10 Feb 2011

**HAL** is a multi-disciplinary open access archive for the deposit and dissemination of scientific research documents, whether they are published or not. The documents may come from teaching and research institutions in France or abroad, or from public or private research centers.

L'archive ouverte pluridisciplinaire **HAL**, est destinée au dépôt et à la diffusion de documents scientifiques de niveau recherche, publiés ou non, émanant des établissements d'enseignement et de recherche français ou étrangers, des laboratoires publics ou privés.

# Time Reversed Absorbing Condition: Application to Inverse Problems

F. Assous\*, M. Kray†, F. Nataf‡, E. Turkel‡

## Abstract

The aim of this paper is to introduce the time-reversed absorbing conditions (*TRAC*) in time-reversal methods. They enable one to “recreate the past” without knowing the source which has emitted the signals that are back-propagated. We present two applications in inverse problems: the reduction of the size of the computational domain and the determination, from boundary measurements, of the location and volume of an unknown inclusion. The method does not rely on any *a priori* knowledge of the physical properties of the inclusion. Numerical tests with the wave and Helmholtz equations illustrate the efficiency of the method. This technique is fairly insensitive with respect to noise in the data.

## Contents

<b>1</b>	<b>Introduction</b>	<b>1</b>
<b>2</b>	<b>The <i>TRAC</i> method and applications</b>	<b>2</b>
2.1	The <i>TRAC</i> method in the time dependent case . . . . .	2
2.2	The <i>TRAC</i> method in the harmonic case . . . . .	5
2.3	Derivation of the <i>TRAC</i> method . . . . .	6
2.4	The wave equation . . . . .	6
2.5	The Helmholtz equation . . . . .	8
2.6	The Maxwell equation . . . . .	8
2.7	Time harmonic Maxwell system . . . . .	10
<b>3</b>	<b>Numerical applications of the <i>TRAC</i> method</b>	<b>10</b>
3.1	The wave equation . . . . .	10
3.2	The Helmholtz equation . . . . .	14
<b>4</b>	<b>Conclusion</b>	<b>18</b>

## 1 Introduction

Since the seminal paper by Fink et al. [FWCM91], time reversal is a subject of very active research. The main idea is to take advantage of the reversibility of wave propagation phenomena, for example in acoustics or electromagnetism in a *non-dissipative* but unknown medium, to back-propagate signals to the sources that emitted them. The initial experiment, see [FWCM91], was to refocus, very precisely, a recorded signal after passing through a barrier consisting of randomly

---

<sup>1</sup>Bar Ilan University, franckassous@netscape.net

<sup>2</sup>University of Paris 6, nataf@ann.jussieu.fr, kray@ann.jussieu.fr

<sup>3</sup>Tel Aviv University, turkel@math.tau.ac.il

distributed metal rods. The remarkable feature of this experiment is the practical possibility to precisely focus a signal after it has crossed random barriers and even without knowing its location. There have been numerous applications of this physical principle, see [Fin09] and references therein. The first mathematical analysis can be found in [BF02] and [BPZ02].

As shown experimentally in [dRF02], it is necessary to know the source that emitted the signals to overcome the diffraction limit. The same difficulty was pointed out in [LMF<sup>+</sup>06] when numerically studying the initial instants of an earthquake by sending back long period time-reversed seismograms.

We will introduce a new method that enables one to “recreate the past” without knowing the source which has emitted the signals that will be back-propagated. This is made possible by using time reversed absorbing conditions (*TRAC*) after removing a small region enclosing the source. This technique has at least two applications in inverse problems:

1. the reduction of the size of the computational domain by redefining the reference surface on which the receivers appear to be located
2. the location of an unknown inclusion from boundary measurements

The first application is reminiscent of the redatuming method introduced in [Ber79]. In our case, we use the wave equation and not a paraxial or parabolic approximation to it. This extends the domain of validity of the redatuming approach. Concerning the second application there is a huge literature that deals with this inverse problem. We mention the MUSIC algorithm [The92] and its application to imaging [LD03], the sampling methods first introduced in [CK96], see the review paper [CCM00] and references therein, and the DORT method [PMSF96]. Mathematical analysis of this kind of approach can be found in [CK98]. These methods were developed in the time-harmonic domain for impenetrable inclusions. The *TRAC* method is designed in both the time-dependent and harmonic domains and does not rely on any *a priori* knowledge of the physical properties of the inclusion. It works both for impenetrable and penetrable inclusions.

The outline of the paper is as follows. In sections 2.1 and 2.2 we introduce the principle of the *TRAC* method both in the time dependent and harmonic domains. We present in section 2.3 two applications of the method in the context of inverse problems. The end of section 2 is devoted to the explicit derivation of the method to the wave and Maxwell equations in both the time dependent and harmonic cases. In section 3 we give numerical applications of the *TRAC* method for the wave equation and the Helmholtz equation. We propose various criteria for applying our method to inverse problems. We investigate the sensitivity with respect to the magnitude of the noise in the data and its ability to handle penetrable inclusions.

## 2 The *TRAC* method and applications

### 2.1 The *TRAC* method in the time dependent case

We consider an incident wave  $U^I$  impinging on an inclusion  $D$  characterized by different physical properties from the surrounding medium. We denote by  $\partial D$  the boundary of this inclusion. The total field  $U^T$  can be decomposed into the incident and scattered field, so  $U^T := U^I + U^S$ . We consider the problem in  $d$  dimensions  $d = 1, 2, 3$  and assume that the total field satisfies a linear hyperbolic equation (or system of equations) denoted by  $\mathcal{L}$ , that can be written

$$\mathcal{L}(U^T) = 0 \text{ in } \mathbf{R}^d \quad (1)$$

together with zero initial conditions, which will be detailed later. The scattering field  $U^S$  has to satisfy a radiation condition at the infinity to ensure the uniqueness of the solution. For

the wave equation we use the Sommerfeld radiation condition, or the Silver-Müller radiation condition for the Maxwell equations (see sections below).

Let  $\Omega$  denote a bounded domain that surrounds  $D$  with  $\Gamma_R$  as its boundary. We assume that the incident wave  $U^I$  has compact support in time and space and that after a time  $T_f$  the total field  $U^T$  vanishes in the bounded domain  $\Omega$ . Let  $V$  be a field that satisfies equation (1). We

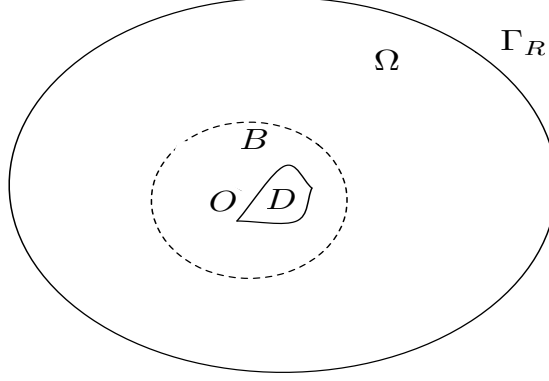


Figure 1: Geometry

denote by  $V_R$  the corresponding time-reversed field that also satisfies the same physical equation. The time-reversed solution  $u_R^T$  of the wave equation (11) is defined by  $u_R^T := u^T(T_f - t, \vec{x})$ , see section 2.4. For the Maxwell equation (24), the time-reversed electromagnetic field is defined by  $(\mathbf{E}_R^T, \mathbf{B}_R^T) := (-\mathbf{E}^T(T_f - t, \vec{x}), \mathbf{B}^T(T_f - t, \vec{x}))$ , see section 2.6. Similar definitions will be used for the incident and scattered fields.

Our first aim is to derive a boundary value problem (BVP) whose solution is the time-reversed field. For this purpose, we assume that we have recorded the value of the total field  $U^T$  on the boundary  $\Gamma_R$  that encloses the domain  $\Omega$ . However, we don't assume to know the physical properties of the inclusion or the exact location of the body i.e. we don't know the exact form of the operator  $\mathcal{L}$  inside the inclusion  $D$ . The only things we know are the physical properties of the surrounding medium, in other words the operator  $\mathcal{L}$  outside  $D$ . There  $\mathcal{L}$  is assumed to be a constant coefficient operator denoted  $\mathcal{L}_0$ . Thus,  $U_R^T$  satisfies the following equation

$$\mathcal{L}_0(U_R^T) = 0 \text{ in } (0, T_f) \times \Omega \setminus D. \quad (2)$$

We impose Dirichlet boundary conditions on  $\Gamma_R$  equal to the time-reversal of the recorded fields and zero initial conditions. The key point is that we lack a boundary condition on the boundary of the inclusion  $\partial D$  in order to define a well-posed BVP on the time-reversed field  $U_R^T$  in  $\Omega \setminus D$ . For inverse problems, the shape and/or location of the inclusion  $D$  is not known and sometimes the type of boundary condition (hard or soft inclusion) on the body is also not known.

To overcome these difficulties, the classical approach for example solves the problem (2) in the entire domain  $\Omega$ , assuming that there is no inclusion  $D$ , see [LMF<sup>+</sup>06] and references therein. Denote by  $W_R^T$  this “approximate” time-reversed solution, we have in the entire domain  $\Omega$ :

$$\mathcal{L}_0(W_R^T) = 0 \text{ in } (0, T_f) \times \Omega \quad (3)$$

with Dirichlet boundary conditions on  $\Gamma_R$  equal to the time reversal of the recorded fields and zero initial conditions. One can readily verify that this approximate time-reversed solution  $W_R^T$  differs from  $U_R^T$ .

**Remark 1** Another possibility is to try to reconstruct the reversed scattered field  $U_R^S$  instead of the total reversed field  $U_R^T$ . In this case, the classical approach consists in solving

$$\mathcal{L}_0(W_R^S) = 0 \text{ in } (0, T_f) \times \Omega$$

with Dirichlet boundary conditions on  $\Gamma_R$  equal to the time reversal of the recorded fields minus the time-reversed incident field and zero initial conditions. It is easy to check that this approximate time-reversed solution  $W_R^S$  differs as well from  $U_R^S$ .

To derive a boundary value problem satisfied by  $U_R^T$  without knowing the physical properties of the inclusion  $D$  or its exact location, we introduce  $B$  a subdomain enclosing the inclusion  $D$ , see Figure 1. Then, we have to determine a specific boundary condition for  $U_R^T$  on the boundary  $\partial B$  so that the solution to this problem will coincide with  $U_R^T$  in the restricted domain  $\Omega \setminus B$ .

In order to derive this boundary condition, we note that  $\mathcal{L}_0(U^I) = 0$  so that the scattered wave  $U^S$  satisfies

$$\begin{cases} \mathcal{L}_0(U^S) = 0 \text{ in } \mathbf{R}^d \setminus D \\ U^S \text{ satisfies a radiation condition at } \infty \end{cases} \quad (4)$$

and zero initial conditions. We make use of the property that the surrounding medium  $\Omega \setminus D$  is homogeneous. As a first step, we look for a relation satisfied by  $U^S$  on  $\partial B$ . Numerical absorbing boundary conditions e.g. [EM77] and [BT80] construct accurate approximations to a perfectly absorbing boundary condition. We denote by ABC an absorbing boundary condition, that can be formally written as

$$\text{ABC}(U^S) = 0 \text{ on } \partial B. \quad (5)$$

Since  $U^T = U^I + U^S$ , we have  $\text{ABC}(U^T - U^I) = 0$  or equivalently  $\text{ABC}(U^T) = \text{ABC}(U^I)$ . Our main ingredient is to *time-reverse* this relation into a relation that we will denote

$$\text{TRAC}(U_R^T) = g(U^I) \text{ on } \partial B \quad (6)$$

where  $g(U^I)$  denotes a known function which is related to the time reversal of  $\text{ABC}(U^I)$ . The design of TRAC and  $g(U^I)$  will be specified in the subsequent sections depending on the specific problem. We shall see that the absorbing boundary condition ABC is different from its time-reverse companion TRAC that will be referred to as a *TRAC* (Time Reversed Absorbing Condition). To summarize, the problem satisfied by  $U_R^T$  in the restricted domain  $\Omega \setminus B$  can be written:

$$\begin{cases} \mathcal{L}_0(U_R^T) = 0 \text{ in } (0, T_f) \times \Omega \setminus B \\ \text{TRAC}(U_R^T) = g(U^I) \text{ on } \partial B \end{cases} \quad (7)$$

together with Dirichlet boundary conditions on  $\Gamma_R$  equal to the time-reversal of the recorded fields and zero initial conditions. By solving (7), we are able to reconstruct the total field  $U^T$  at any point of the domain  $\Omega \setminus B$  and any time in  $(0, T_f)$ .

We shall illustrate our approach by deriving equation (7) from equation (4) for several classical examples: the wave equation and the Maxwell system. The same procedure can be applied to the elasticity system and *non-linear* hyperbolic problems before a shock formation.

## 2.2 The *TRAC* method in the harmonic case

We consider the time-harmonic counterpart of problem (1) and denote by  $\widehat{\mathcal{L}}$  the Fourier transform in time of the operator  $\mathcal{L}$ . The unknown total field  $\mathbf{U}^T(\vec{x})$  is decomposed into the sum of an incident field  $\mathbf{U}^I(\vec{x})$  and of a scattered field  $\mathbf{U}^S(\vec{x})$ . We have:

$$\begin{cases} \widehat{\mathcal{L}}(\mathbf{U}^T) = 0 \text{ in } \mathbf{R}^d \\ \mathbf{U}^S(\vec{x}) := \mathbf{U}^T(\vec{x}) - \mathbf{U}^I(\vec{x}) \text{ satisfies a Sommerfeld condition at } \infty. \end{cases} \quad (8)$$

In this context, the analog to the time-reversal method is the phase conjugation technique, see [CM91]. Let  $\mathbf{V}$  be a field that satisfies the harmonic equation. We denote by  $\mathbf{V}_R$  the corresponding *harmonic time-reversed* field that still satisfies the same harmonic equation. For the Helmholtz equation (21) we proceed in the following way. Let  $v(t, \vec{x})$  be a time dependent real valued function solution to the wave equation and  $v_R(t, \vec{x}) := v(-t, \vec{x})$  its associated time-reversed function. Since we consider the harmonic case, there is no notion of a final time  $T_f$  as above. The Fourier transform in time of the above definition yields:

$$\widehat{v}_R(\omega, \vec{x}) = \int v(-t, \vec{x}) e^{-i\omega t} dt = \int v(t, \vec{x}) e^{i\omega t} dt = \overline{\int v(t, \vec{x}) e^{-i\omega t} dt} = \overline{\widehat{v}(\omega, \vec{x})}.$$

This identity shows that the phase conjugation is the Fourier transform of the time-reversal process in the case of the Helmholtz equation. For the harmonic Maxwell equation (31), we proceed in a slightly different way. Recall that for the Maxwell equation (24), the time-reversed electromagnetic field was defined by  $(\mathbf{E}_R, \mathbf{B}_R) := (-\mathbf{E}(-t, \vec{x}), \mathbf{B}(-t, \vec{x}))$ , see section 2.6. The Fourier transform in time of the above definition yields:

$$(\widehat{\mathbf{E}}_R(\omega, \vec{x}), \widehat{\mathbf{B}}_R(\omega, \vec{x})) = (-\overline{\widehat{\mathbf{E}}(\omega, \vec{x})}, \overline{\widehat{\mathbf{B}}(\omega, \vec{x})}).$$

Thus, the classical *time-reversal* process in the harmonic regime applied to (8) amounts to conjugating the recorded data (and in the Maxwell case to take the opposite of the electric field) and solving the following harmonic time-reversed problem:

$$\begin{cases} \widehat{\mathcal{L}}_0(\mathbf{W}_R^T) = 0 \text{ in } \Omega \\ \mathbf{W}_R^T = \mathbf{U}_R^T \text{ on } \Gamma_R \end{cases} \quad (9)$$

which is the equivalent to (3) in the harmonic regime. Hence, following the same steps as above for deriving equation (7) from equation (1), we get:

$$\begin{cases} \widehat{\mathcal{L}}_0(\mathbf{U}_R^T) = 0 \text{ in } \Omega \setminus B \\ \text{TRAC}(\mathbf{U}_R^T) = \widehat{g(\mathbf{U}^I)} \text{ on } \partial B \end{cases} \quad (10)$$

together with Dirichlet boundary conditions on  $\Gamma_R$  equal to the harmonic time-reverse of the recorded fields.

We shall illustrate our approach by deriving equation (10) for several classical examples: the Helmholtz equation and the *time harmonic* Maxwell system. The same process can be applied to the *time harmonic* elasticity system.

### 2.3 Derivation of the *TRAC* method

A first application to inverse problems is a reduction of the size of the computational domain. Since, we are able to compute the total field  $U^T$  on an artificial boundary  $\partial B$ , it is equivalent to having the boundary  $\Gamma_R$  moved to  $\partial B$ . As a consequence, the cost of the forward problems involved in the identification algorithm is reduced.

A second application is to localize the inclusion by a trial and error procedure. At the initial time  $t = 0$ , the total field  $U^T$  is zero. Thus, if  $B$  encloses the inclusion  $D$ ,  $U_R^T$  which is exactly the time-reversal of  $U^T$  is zero at the final time  $T_f$  that corresponds to the initial time of the physical problem (1). Conversely, if after solving equation (7),  $U_R^T$  is not zero at the final time  $T_f$ , it proves that the assumption that  $D$  is a subset of  $B$  is false. Hence, by playing with the location and size of the subdomain  $B$ , it could be possible to determine the location and volume of the inclusion  $D$ . This technique will be the core subject of section 3.

### 2.4 The wave equation

We first consider the case of the three dimensional acoustic wave equation with a propagation speed  $c$  which is constant outside an inclusion  $D$ . We denote the total field as  $u^T$  which is decomposed into an incident  $u^I$  and a scattered field  $u^S$ . With these notations, equation (4) reads:

$$\begin{cases} \frac{\partial^2 u^S}{\partial t^2} - c^2 \Delta u^S = 0 \text{ in } \mathbf{R}^3 \setminus D \\ u^S(t, \vec{x}) \text{ satisfies a Sommerfeld condition at } \infty \\ \text{homogeneous initial conditions.} \end{cases} \quad (11)$$

This problem is under-determined since we don't specify any boundary condition on  $\partial D$ . Thus  $u^S$  is not necessarily zero. We define the time-reversed total field  $u_R^T$  by  $u_R^T(t, \cdot) := u^T(T_f - t, \cdot)$ . Since, the wave equation involves only second order time derivatives, this definition ensures that the reverse field  $u_R^T$  is a solution to the wave equation as well. In order to derive the absorbing boundary condition (5), we consider, for the sake of simplicity, that the subdomain  $B$  is a ball of radius  $\rho$  centered at the origin denoted  $B_\rho$ . Let  $r$  be the radial coordinate, we consider the first order Bayliss-Turkel *ABC BT*<sup>1</sup> [BT80, BGT82]:

$$\frac{\partial u^S}{\partial t} + c \frac{\partial u^S}{\partial r} + c \frac{u^S}{r} = 0. \quad (12)$$

For ease of the derivation in three dimensions, we use an equivalent form of equation (12):

$$\frac{\partial}{\partial t}(ru^S) + c \frac{\partial}{\partial r}(ru^S) = 0. \quad (13)$$

The above equation is the counterpart of equation (5) for the wave equation. We next wish to express (6) explicitly for the time-reversed equation (13). The total field  $u^T = u^I + u^S$  satisfies

$$\frac{\partial}{\partial t}(ru^T(t, \cdot)) + c \frac{\partial}{\partial r}(ru^T(t, \cdot)) = \frac{\partial}{\partial t}(ru^I(t, \cdot)) + c \frac{\partial}{\partial r}(ru^I(t, \cdot)).$$

Using  $u_R^T(t, \cdot) = u^T(T_f - t, \cdot)$ , we get

$$(-\frac{\partial}{\partial t}(ru_R^T) + c \frac{\partial}{\partial r}(ru_R^T))|_{T_f-t} = \frac{\partial}{\partial t}(ru^I(t, \cdot)) + c \frac{\partial}{\partial r}(ru^I(t, \cdot)),$$

or equivalently,

$$-\frac{\partial}{\partial t}(r u_R^T(t, \cdot)) + c \frac{\partial}{\partial r}(r u_R^T(t, \cdot)) = (\frac{\partial}{\partial t}(r u^I) + c \frac{\partial}{\partial r}(r u^I))|_{T_f - t}.$$

Note, that on  $\partial B_\rho$ ,  $\partial / \partial r = -\partial / \partial n$  where  $n$  is the outward normal to the restricted domain  $\Omega \setminus B_\rho$ . Multiplying by  $-1$ , we get

$$\frac{\partial}{\partial t}(r u_R^T(t, \cdot)) + c \frac{\partial}{\partial n}(r u_R^T(t, \cdot)) = -(\frac{\partial}{\partial t}(r u^I) - c \frac{\partial}{\partial n}(r u^I))|_{T_f - t}. \quad (14)$$

Another way to write this boundary condition is to introduce the time-reversed incident field

$$u_R^I(t, \cdot) := u^I(T_f - t, \cdot),$$

so that (14) can be expressed as

$$\frac{\partial}{\partial t}(r u_R^T(t, \cdot)) + c \frac{\partial}{\partial n}(r u_R^T(t, \cdot)) = \frac{\partial}{\partial t}(r u_R^I(t, \cdot)) + c \frac{\partial}{\partial n}(r u_R^I(t, \cdot)). \quad (15)$$

This expression is the counterpart of equation (6). Since  $\partial r / \partial n = -1$ , relation (15) can be rewritten as:

$$\frac{\partial}{\partial t}(u_R^T(t, \cdot)) + c \frac{\partial}{\partial n}(u_R^T(t, \cdot)) - c \frac{u_R^T(t, \cdot)}{r} = \frac{\partial}{\partial t}(u_R^I(t, \cdot)) + c \frac{\partial}{\partial n}(u_R^I(t, \cdot)) - c \frac{u_R^I(t, \cdot)}{r}. \quad (16)$$

So we define the boundary condition TRAC by:

$$\text{TRAC}(u_R^T) := \frac{\partial}{\partial t}(u_R^T(t, \cdot)) + c \frac{\partial}{\partial n}(u_R^T(t, \cdot)) - c \frac{u_R^T(t, \cdot)}{r}. \quad (17)$$

Note, that due to the minus sign before the term  $u_R^T/r$ , the *TRAC* (16) is *not* the  $BT^1$  absorbing boundary condition. The time-reversed problem analog to (7) reads:

$$\left\{ \begin{array}{l} \frac{\partial^2 u_R^T}{\partial t^2} - c^2 \Delta u_R^T = 0 \text{ in } (0, T_f) \times \Omega \setminus B_\rho \\ \text{TRAC}(u_R^T) = \text{TRAC}(u_R^I) \text{ on } \partial B_\rho \\ u_R^T(t, \vec{x}) = u^T(T_f - t, \vec{x}) \text{ on } \Gamma_R \\ \text{zero initial conditions.} \end{array} \right. \quad (18)$$

The *TRAC* is not only not the standard  $BT^1$  *ABC* but also has an “anti absorbing” term ( $-cu_R^T/r$ ). A natural concern arises about the well-posedness of *BVP* (18). Although we have not developed a general theory, we prove an energy estimate for this problem in a special geometry, see [AKNT10]. In many computations we have never encountered stability problems. In section 3 a numerical procedure for inclusion identification will be deduced from this formulation.

The generalization of (17) to two space dimensions is straightforward, see [BT80, BGT82]. In the above computation, it is sufficient to replace  $r$  by  $\sqrt{r}$  and  $1/r$  by  $1/(2r)$  and (17) reads:

$$\frac{\partial u^S}{\partial t} + c \frac{\partial u^S}{\partial r} + c \frac{u^S}{2r} = 0. \quad (19)$$

In the above derivation we have assumed that the surface  $B$  is a sphere or a circle. Since we are finding an approximate location of the inclusion this is usually sufficient. For an elongated



body a ball can be replaced by an ellipse or spheroidal surface. Absorbing boundary conditions for these cases have been developed in [MTH08, MT09, BDSG09]. For more general surfaces several absorbing conditions have been developed, for example [ABB99, KTU87]. Comparisons between many options are presented in [MTH08, MT09]. As shown above, a first order *TRAC* method simply reverses the sign of the non-differentiated term of the corresponding first order absorbing boundary condition. Thus, a first order *TRAC* for a general bounding surface in two dimensions is given by:

$$\text{TRAC}(u_R^T) := \frac{\partial}{\partial t}(u_R^T(t, \cdot)) + c \frac{\partial}{\partial n}(u_R^T(t, \cdot)) - \frac{c\kappa}{2} u_R^T(t, \cdot) \quad (20)$$

where  $\kappa$  is the curvature of the bounding surface  $B$ .

## 2.5 The Helmholtz equation

Denote by  $\omega$  the dual variable of  $t$  for the Fourier transform in time. The total field  $u^T$  can be decomposed into an incident and scattered field, i.e.  $u^T := u^I + u^S$ . The Helmholtz equation is derived by taking the Fourier transform in time of the wave equation, yielding:

$$\begin{cases} -\omega^2 u^T - c^2 \Delta u^T = 0 \text{ in } \mathbf{R}^3 \\ (u^T - u^I) \text{ satisfies a Sommerfeld radiation condition at } \infty. \end{cases} \quad (21)$$

Recall that our aim is to write a *BVP* whose solution is the conjugate of  $u^T$ . Following section 2.2, it is sufficient to take the Fourier transform of equation (18) to get:

$$\begin{cases} -\omega^2 u_R^T - c^2 \Delta u_R^T = 0 \text{ in } \Omega \setminus B_\rho \\ i\omega u_R^T + c \frac{\partial u_R^T}{\partial n} - c \frac{u_R^T}{r} = i\omega u_R^I + c \frac{\partial u_R^I}{\partial n} - c \frac{u_R^I}{r} \text{ on } \partial B_\rho \\ u_R^T(\vec{x}) = \bar{u}^T(\vec{x}) \text{ on } \Gamma_R. \end{cases} \quad (22)$$

We emphasize that the time-reversed absorbing condition *TRAC*

$$\text{TRAC}(u_R^T) := i\omega u_R^T + c \frac{\partial u_R^T}{\partial n} - c \frac{u_R^T}{r} = \text{given} \quad (23)$$

is not the  $BT^1$  absorbing boundary condition

$$i\omega u^T + c \frac{\partial u^T}{\partial n} + c \frac{u^T}{r} = \text{given}.$$

As before, generalizations to two dimensions and other shapes for  $B$  are straightforward.

## 2.6 The Maxwell equation

As a second case, we consider the three dimensional Maxwell equations. For the sake of simplicity, we assume that outside the inclusion  $D$  the medium is linear, homogeneous and isotropic with a constant speed of light denoted by  $c$ . Denote by  $\mathbf{E}$  the electric field and by  $\mathbf{B}$  the magnetic induction. Denote the total field by  $(\mathbf{E}^T, \mathbf{B}^T)$  which is decomposed as above into

an incident  $(\mathbf{E}^I, \mathbf{B}^I)$  and a scattered field  $(\mathbf{E}^S, \mathbf{B}^S)$ . With these notations, the counterpart of equation (4) reads

$$\left\{ \begin{array}{l} \frac{\partial \mathbf{E}^S}{\partial t} - c^2 \nabla \times \mathbf{B}^S = 0, \text{ in } \mathbf{R}^3 \setminus D, \\ \frac{\partial \mathbf{B}^S}{\partial t} + \nabla \times \mathbf{E}^S = 0, \text{ in } \mathbf{R}^3 \setminus D, \\ (\mathbf{E}^S(t, \vec{x}), \mathbf{B}^S(t, \vec{x})) \text{ satisfies a Silver - Müller radiation condition at } \infty \\ \text{and zero initial conditions.} \end{array} \right. \quad (24)$$

We introduce the time-reversed solution

$$(\mathbf{E}_R^T(t, \vec{x}), \mathbf{B}_R^T(t, \vec{x})) := (-\mathbf{E}(T_f - t, \vec{x}), \mathbf{B}(T_f - t, \vec{x})). \quad (25)$$

Note, that the Maxwell system is a first order hyperbolic system, but is not invariant under a time-reversal. So, we multiply the electric field by  $(-1)$  so that the electromagnetic field  $(\mathbf{E}_R^T(t, \vec{x}), \mathbf{B}_R^T(t, \vec{x}))$  solves a time-reversible equation and we can construct an absorbing boundary condition analog to (5). We still consider a subdomain  $B$  that is a ball of radius  $\rho$  centered at the origin and denoted  $B_\rho$ . We assume that the following approximate absorbing Silver-Müller boundary condition is reasonable:

$$(\mathbf{E}^S \times \nu) \times \nu + c \mathbf{B}^S \times \nu = 0 \quad (26)$$

where  $\nu$  is the outward normal to the ball  $B_\rho$ . The above equation is the counterpart of equation (5) for the Maxwell equation. The next step is to derive an explicit expression for the time reverse of equation (26). This means that the total field satisfies

$$(\mathbf{E}^T \times \nu) \times \nu + c \mathbf{B}^T \times \nu = (\mathbf{E}^I \times \nu) \times \nu + c \mathbf{B}^I \times \nu. \quad (27)$$

Using definition (25), we get

$$(-\mathbf{E}_R^T \times \nu) \times \nu + c \mathbf{B}_R^T \times \nu = \left( (\mathbf{E}^I \times \nu) \times \nu + c \mathbf{B}^I \times \nu \right)_{T_f - t}. \quad (28)$$

Note, that on  $\partial B_\rho$ ,  $n = -\nu$  and multiplying by  $-1$ , we get

$$(\mathbf{E}_R^T \times n) \times n + c \mathbf{B}_R^T \times n = - \left( (\mathbf{E}^I \times \nu) \times \nu + c \mathbf{B}^I \times \nu \right)_{T_f - t}. \quad (29)$$

This expression is the counterpart of (6). Finally, the time-reversed problem analog to (7) reads:

$$\left\{ \begin{array}{l} \frac{\partial \mathbf{E}_R^T}{\partial t} - c^2 \nabla \times \mathbf{B}_R^T = 0, \text{ in } \Omega \setminus B_\rho, \\ \frac{\partial \mathbf{B}_R^T}{\partial t} + \nabla \times \mathbf{E}_R^T = 0, \text{ in } \Omega \setminus B_\rho, \\ (\mathbf{E}_R^T \times n) \times n + c \mathbf{B}_R^T \times n = - \left( (\mathbf{E}^I \times \nu) \times \nu + c \mathbf{B}^I \times \nu \right)_{T_f - t} \text{ on } \partial B_\rho \\ (\mathbf{E}_R^T(t, \vec{x}), \mathbf{B}_R^T(t, \vec{x})) = (-\mathbf{E}(T_f - t, \vec{x}), \mathbf{B}(T_f - t, \vec{x})) \text{ on } \Gamma_R \\ \text{and zero initial conditions.} \end{array} \right. \quad (30)$$

The penultimate equation in the above system expresses that we have time-reversed the data recorded on  $\Gamma_R$ .

## 2.7 Time harmonic Maxwell system

We again, denote by  $\omega$  the dual variable of  $t$  for the Fourier transform in time. The total field  $(\mathbf{E}^T(\vec{x}), \mathbf{B}^T(\vec{x}))$  can be decomposed into an incident and scattered field,  $(\mathbf{E}^T(\vec{x}), \mathbf{B}^T(\vec{x})) := (\mathbf{E}^I(\vec{x}), \mathbf{B}^I(\vec{x})) + (\mathbf{E}^S(\vec{x}), \mathbf{B}^S(\vec{x}))$ . The time-harmonic Maxwell equation is written by taking the Fourier transform in time of the Maxwell equation:

$$\begin{cases} i\omega \mathbf{E}^T - c^2 \nabla \times \mathbf{B}^T = 0, & \text{in } \mathbf{R}^3, \\ i\omega \mathbf{B}^T + \nabla \times \mathbf{E}^T = 0, & \text{in } \mathbf{R}^3, \\ (\mathbf{E}^T, \mathbf{B}^T) - (\mathbf{E}^I, \mathbf{B}^I) \text{ satisfies a Silver - Müller radiation condition at } \infty. \end{cases} \quad (31)$$

Recall that our aim is to write a *BVP* whose solution is the harmonic time reverse of  $(\mathbf{E}^T(\vec{x}), \mathbf{B}^T(\vec{x}))$ . Following 2.2, it is sufficient to take the Fourier transform of equation (30) to get

$$\begin{cases} i\omega \mathbf{E}_R^T - c^2 \nabla \times \mathbf{B}_R^T = 0, & \text{in } \Omega \setminus B_\rho, \\ i\omega \mathbf{B}_R^T + \nabla \times \mathbf{E}_R^T = 0, & \text{in } \Omega \setminus B_\rho, \\ (\mathbf{E}_R^T \times \mathbf{n}) \times \mathbf{n} + c \mathbf{B}_R^T \times \mathbf{n} = - \left( (\bar{\mathbf{E}}^I \times \nu) \times \nu + c \bar{\mathbf{B}}^I \times \nu \right) & \text{on } \partial B_\rho \\ (\mathbf{E}_R^T(\vec{x}), \mathbf{B}_R^T(\vec{x})) = (-\bar{\mathbf{E}}(\vec{x}), \bar{\mathbf{B}}(\vec{x})) & \text{on } \Gamma_R. \end{cases} \quad (32)$$

## 3 Numerical applications of the *TRAC* method

In section 3.1, we describe the *TRAC* method to locate a scatterer in the two-dimensional case together with computational results. We first consider the time-dependent wave equation. The Helmholtz equation will be studied in 3.2. As explained in section 2.1, the method does not rely on any *a priori* knowledge of the physical properties of the inclusion. We will treat, in the same manner, the cases of a hard, soft or penetrable inclusion. In the harmonic case, we compare the *TRAC* approach with the phase conjugation approach presented in (9).

### 3.1 The wave equation

We consider an inclusion  $D$  surrounded by a homogeneous and isotropic medium with a velocity of sound denoted by  $c_0$ . The scatterer is illuminated by an incident field  $u^I$ . Equation (1) reads:

$$\begin{cases} \frac{\partial^2 u^T}{\partial t^2} - c^2 \Delta u^T = 0 & \text{in } \mathbf{R}^2 \\ (u^T(t, \vec{x}) - u^I(t, \vec{x})) \text{ satisfies a Sommerfeld condition at } \infty \\ \text{zero initial conditions.} \end{cases} \quad (33)$$

In order to create synthetic data, equation (33) is approximated by the FreeFem++ package [Hec10] which implements a finite element method in space. In the paper the small size of the domain enables us to use a standard  $P^1$  finite element method. The advancement in time is given by a second order central finite difference scheme so that it is time reversible also on the numerical level. The computational domain is truncated by using an absorbing boundary condition. The incident wave is simulated by the same procedure with a uniform velocity of

sound,  $c_0$ . We introduce a boundary  $\Gamma_R$  where the signal is recorded. The boundary  $\Gamma_R$  encloses a domain denoted  $\Omega$ , see Fig. 1. The next stage of the method is to introduce a “trial” domain  $B_\rho$  and solve the time-reversed problem (18) in  $\Omega \setminus B_\rho$ .

*The principle of the method (see section 2.3) is that when the ball  $B_\rho$  encloses the inclusion  $D$  then, at the final time of the reverse simulation, the solution must be equal to the initial condition of the forward problem i.e. zero. Conversely, if at the end of the reverse simulation the field is not zero, it shows that the ball  $B_\rho$  does not enclose the inclusion  $D$ .*

As a first test case, we consider an inclusion that is a soft disk and  $B_\rho$  is a disk of variable radius. In Fig. 2, we have several lines and three columns. Each column corresponds to a numerical time-reversed experiment and each line corresponds to a snapshot of the solution at a given time. The top line corresponds to the initial time for the time-reversed problem, equivalent to  $t = T_f$  for the forward problem. The last line is the solution at the final time of the reversed simulation which corresponds to the initial time  $t = 0$  for the forward problem. In the left column, we display the perfect time reverse solution which is the reverse of the forward problem. For the inverse problem, the data is not known. It is shown for reference only.

In the middle column, we display the solution of the reversed problem (18) with a ball  $B_\rho$  which encloses the inclusion. As expected, the sequence of snapshots is the restriction to the domain  $\Omega \setminus B_\rho$  of the left column. This exemplifies one application of the *TRAC* method: if we know that the ball  $B_\rho$  encloses the inclusion we are able to reconstruct the signal in a region that is closer to the inclusion than the line of receivers  $\Gamma_R$ . This allows the reduction of the size of the computational domain. In this respect, the method is related to the redatuming method, see [Ber79]. In the last column we show the solution of the reversed problem (18) with a ball  $B_\rho$  smaller than the soft disk. In contrast to the previous case, the sequence of snapshots differs from the left column.

For the inverse problem of locating the scatterer, we only know that at the final time the solution should be zero. In the middle column, this criterion is satisfied and we can thus infer that the inclusion  $D$  is included in the ball  $B_\rho$ . On the other hand, when the final solution in the last column is not zero it shows that  $D$  is not included in the ball  $B_\rho$ . This observation leads to an easy to compute criterion which is independent of the size of the domain:

$$J(B_\rho) := \frac{\|u_R^T(T_f, \cdot)\|_{L^\infty(\Omega \setminus B_\rho)}}{\sup_{t \in [0, T_f]} \|u^I(t, \cdot)\|_{L^\infty(\Omega)}} \quad (34)$$

which vanishes when the artificial ball encloses the inclusion. Due to numerical errors and the fact that the *TRAC* is not an exact *ABC*, the criterion is small but not zero, see Fig. 5.

Inverse problems are frequently ill-posed. Hence, a crucial question is the sensitivity of the method with respect to noise in the data. Therefore, we shall add Gaussian noise by replacing the recorded data  $u^T$  on  $\Gamma_R$  by

$$u^T := (1. + Coeff * (-1. + 2. * randn)) * u^T, \quad (35)$$

where *randn* satisfies a centered reduced normal law and *Coeff* is the level of noise. The solutions at the final time are depicted on Fig. 3. The level of noise is between 10% and 50%. On the top line we display the results for a ball larger than the inclusion. Due to the noise, the final solution is no longer zero but is a random signal of size related to the level on noise. In the bottom line we display the result when the ball is smaller than the inclusion. Now, together with a random signal there appears a structured non-zero solution which looks like the right column of Fig. 2 without noise in the data. We can discriminate between the case where the ball contains or does not contain the inclusion  $D$  up to 45% of noise. Indeed in this case,  $J(B_\rho) = 0.2$

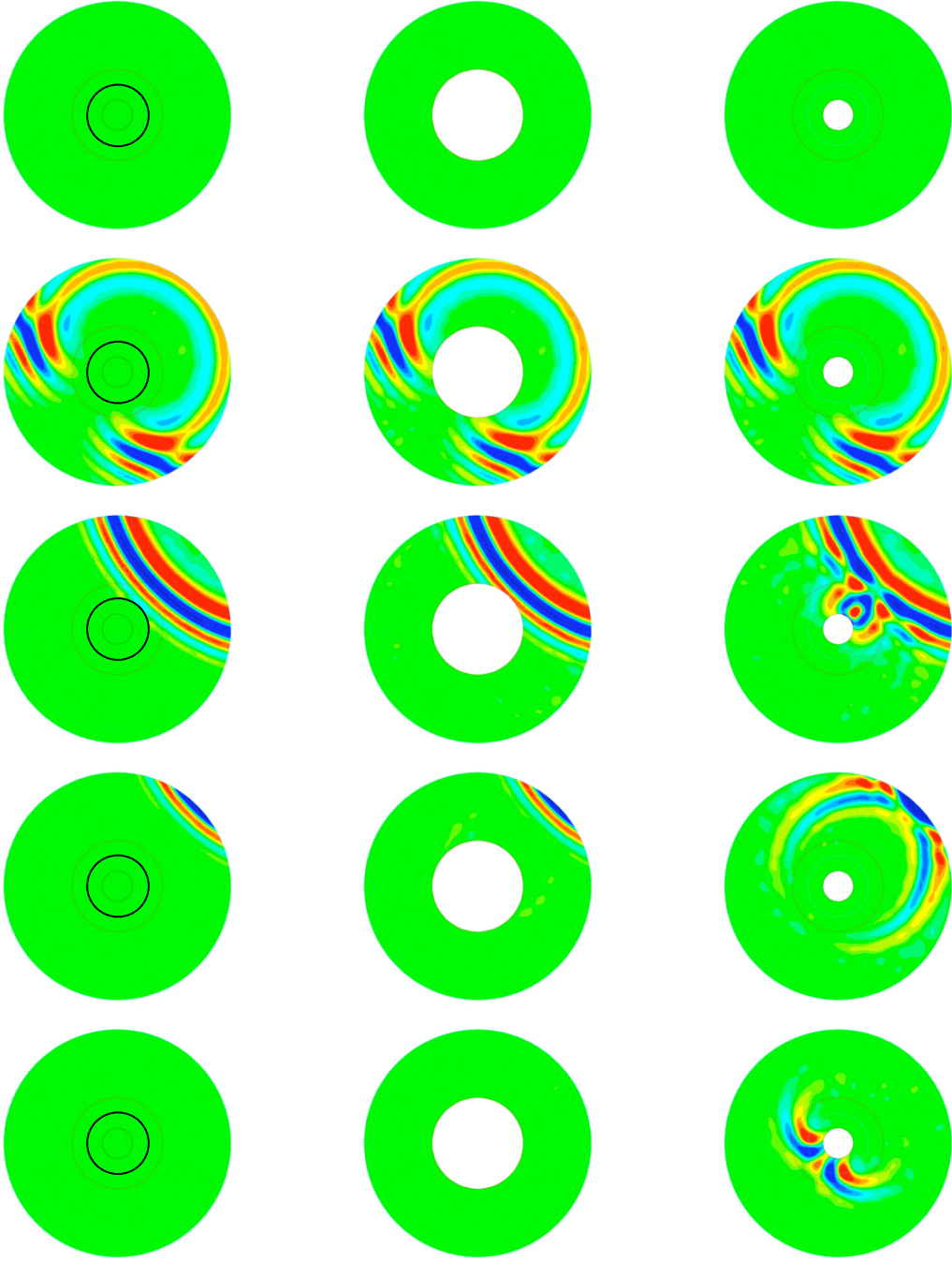


Figure 2: Time reversed BVP snapshots for a soft inclusion with an incident signal of the forward problem (not shown here) coming from the top-right. On the left: perfect time-reversed solution, in the middle: time-reversal with larger ball, on the right: time-reversal with a smaller ball.

so the magnitude of the final solution is 20% of the incident field when the ball  $B_\rho$  encloses the inclusion whereas  $J(B_\rho) = 0.6$  when the ball does not enclose the inclusion. Thus, the method *TRAC* appears to be relatively insensitive to noise on the recorded data.

In the previous tests, for the sake of simplicity, the artificial balls and the inclusion were

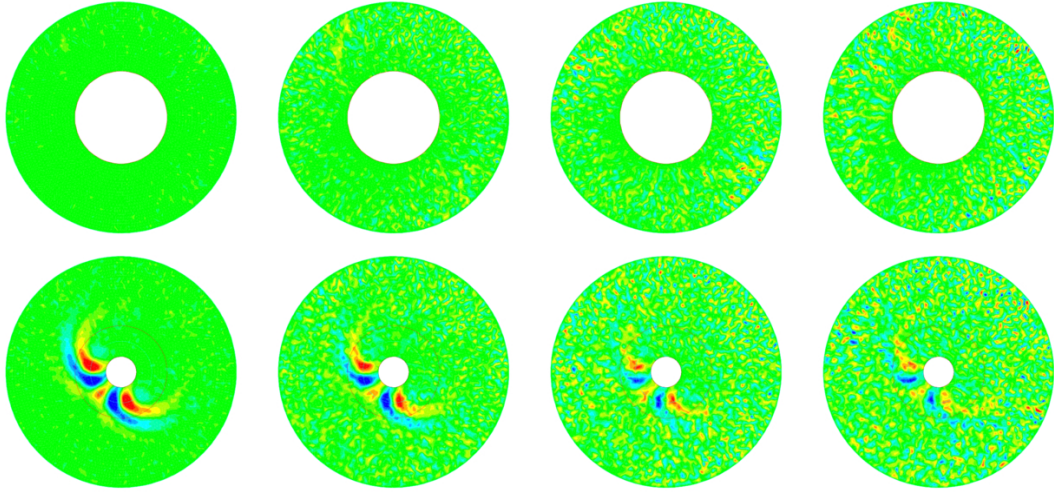


Figure 3: Time reversed solutions at the final time for noise on the recorded data from left to right: 10%, 30%, 45% and 50%, for a ball larger than the inclusion on the top and a smaller ball on the bottom

concentric. We now consider the case where either the artificial ball and the inclusion  $D$  do not intersect or the artificial ball crosses  $D$  without including or being included, see Fig. 4. Results are shown in Tables 1 and 2. In Table 1, the inclusion is between the artificial boundaries. Since in our tests the source emits from the North-East, we place the inclusion respectively in North-East, North-West, South-West and South-East for Table 2. The radius of the inclusion is  $1.35\lambda$ , the radius of the larger ball is about  $3\lambda$  and the radius of the smaller one is always  $\lambda$ . In all these cases, the criterion  $J(B_\rho)$  discriminates between the possibilities since it takes values smaller than 0.05 when the artificial ball encloses the inclusion whereas it lies between 0.3 and 1.0 in the other cases. Moderate values of the criterion ( $J(B_\rho) = 0.3$ ) correspond to a situation where the inclusion is in the shadow of the ball.

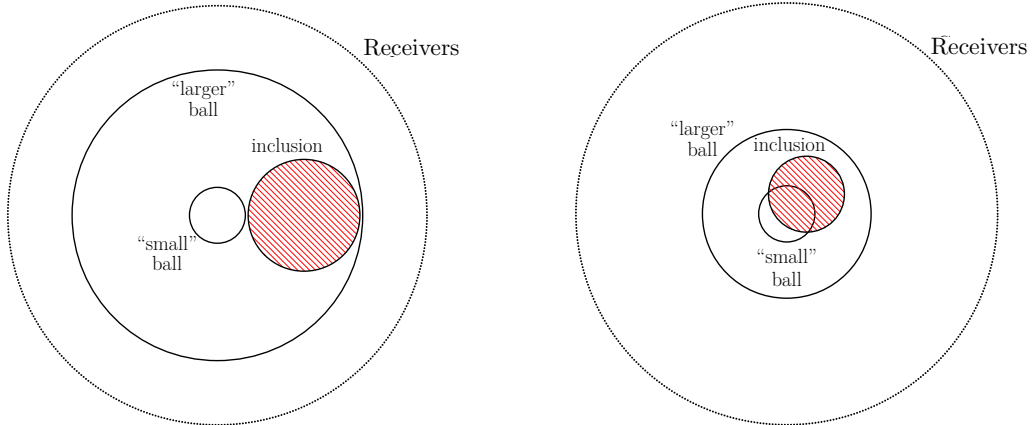


Figure 4: (a) Inclusion between the artificial boundaries (b) Inclusion crossing the artificial boundaries.

As a second test case we illustrate the *TRAC* method by taking penetrable inclusions with speeds that correspond to medical applications. The values of the speed in the inclusion are taken

radius inclusion	radius large ball	radius small ball	Results for large ball	Results for small ball
$2\lambda$	$5.2\lambda$	$\lambda$	$< 5\%$	100%
$\lambda$	$5.2\lambda$	$\lambda$	$< 5\%$	100%
$\lambda$	$3.2\lambda$	$\lambda$	$< 5\%$	100%
$0.5\lambda$	$5.2\lambda$	$\lambda$	$< 5\%$	50%
$0.5\lambda$	$2.2\lambda$	$\lambda$	$< 5\%$	50%

Table 1: Results of  $J(B_\rho)$  for inclusions that do not intersect the artificial balls, see Fig. 4 (a).

Geographical position	Results for large ball	Results for small ball
N-E	$< 5\%$	65%
N-W	$< 5\%$	70%
S-W	$< 5\%$	30%
S-E	$< 5\%$	75%

Table 2: Results of  $J(B_\rho)$  for an inclusion crossing the artificial balls, see Fig. 4 (b)

from [STX<sup>+</sup>05]:  $c = 1.7$  (breast tumor),  $c = 1.14$  (fibroadenoma) and  $c = 0.93$  (surrounding tissue). We again stress that the method does not rely on any a priori knowledge of the data. For these inclusions, the ball and the inclusion are concentric disks and we vary the size of the artificial balls. In Fig. 5, we plot the criterion  $J(B_\rho)$  as a function of the distance between the inclusion and the artificial balls for various penetrable bodies. When the abscissa is negative, the ball does not enclose the inclusion.  $J(B_\rho)$  is even larger when the ball is smaller than the inclusion. The criterion increases with the distance between the ball and the inclusion. On the other hand, when the ball encloses the inclusion (i.e. the abscissa is positive) the criterion is smaller than 0.1 and nearly flat. Note, that as expected, the larger the contrast between the inclusion and the surrounding medium the larger is  $J(B_\rho)$ . We have done other experiments with inclusions of various shapes. One such example is given later for the Helmholtz equation. In all cases, the results are independent of the shape of the inclusion as long as its size is greater than one wavelength.

In conclusion, when we enclose the body with  $B_\rho$  then  $J(B_\rho)$  is small. When the ball does not include the body  $D$  then the size of  $J(B_\rho)$  indicates the distance between the scatterer and the artificial ball.

### 3.2 The Helmholtz equation

For the harmonic case, we again consider a scatterer  $D$  surrounded by a homogeneous and isotropic medium with a velocity of sound denoted by  $c_0$ . The inclusion is illuminated by an incident field  $u^I$ . Equation (8) becomes:

$$\begin{cases} -\omega^2 u^T - c^2 \Delta u^T = 0 \text{ in } \mathbf{R}^2 \\ (u^T(\vec{x}) - u^I(\vec{x})) \text{ satisfies a Sommerfeld condition at } \infty. \end{cases} \quad (36)$$

In order to create synthetic data, equation (36) is approximated by the FreeFem++ package [Hec10] which constructs a finite element method in space. The computational domain is truncated by using an absorbing boundary condition. The incident wave is simulated by the

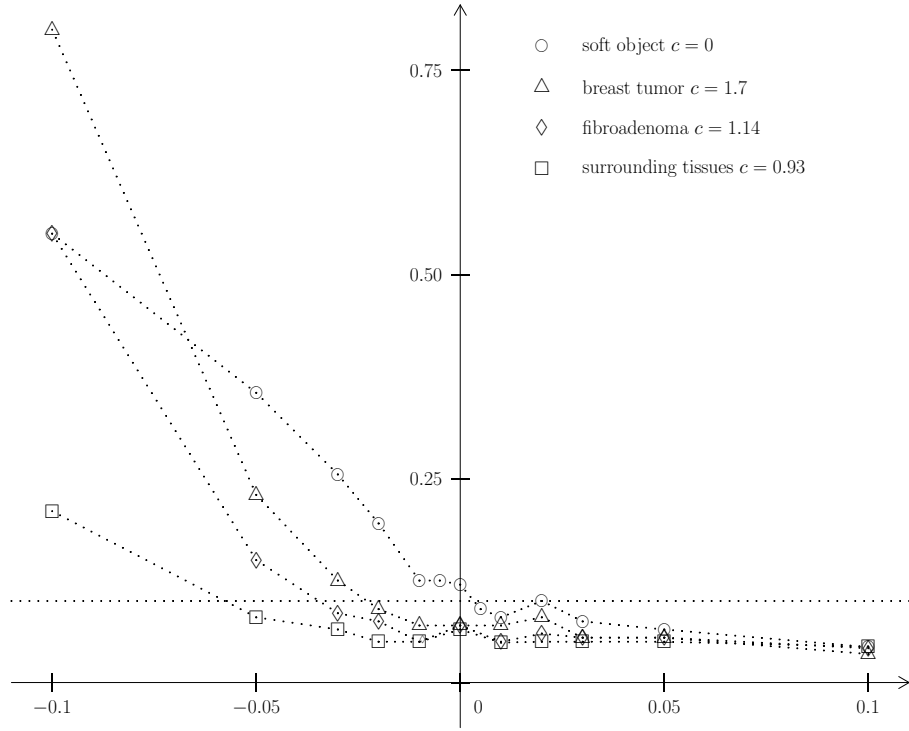


Figure 5: Criterion  $J(B_\rho)$  vs. the algebraic distance between the inclusion and the artificial balls for various penetrable inclusions

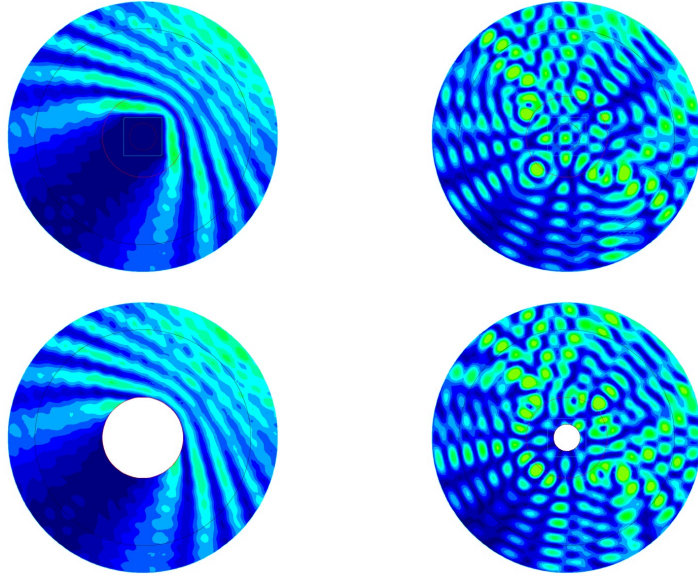


Figure 6: Phase conjugation for a soft square shaped inclusion of length  $2\lambda$ . From left to right, from top to bottom : perfect, phase conjugation, *TRAC* with a ball enclosing the inclusion, *TRAC* with a ball inside the inclusion.



same procedure with a uniform velocity of sound equal to  $c_0$ . We then introduce a boundary  $\Gamma_R$  where the signal is recorded. The boundary  $\Gamma_R$  encloses a domain denoted  $\Omega$ , see Fig. 1. The next stage of the method is to introduce a “trial” domain  $B_\rho$  and solve the phase conjugated problem (22) in  $\Omega \setminus B_\rho$ . In contrast to the time dependent case, we cannot use the criterion defined in (34) since in the harmonic case, there is no time and thus no final time. We define, later, two new criteria adapted to the harmonic case. We first look at the numerical simulations obtained with artificial balls and a soft square shaped inclusion that are concentric, see Fig. 6. On the top left figure we plot the modulus of the total field  $|u^T|$  which coincides with the modulus of its conjugate field  $|\bar{u}^T|$ . On the right, we display the field obtained by the phase-conjugation method presented in section 2.2, see equation (9). We see that there is a large difference between the total field and the field reconstructed by the phase conjugation method. The two bottom figures illustrate the *TRAC* method. On the left figure, the ball encloses the square and the computed field is the restriction of the total field. On the right figure, the ball is inside the square and the computed field is very different from the total field.

In practice, we don’t know the total field and we have to introduce a way to measure whether the artificial ball encloses the inclusion or not. For this purpose, we introduce two different criteria. The first one is based on Dirichlet and Neumann data and the second one is based on the use of absorbing boundary conditions. The latter will prove to be more robust with respect to noise without requiring regularization techniques. For the first criterion, we assume that in addition to the total field  $u^T$  we have also recorded the value of the normal derivative  $\partial u^T / \partial n$  on the boundary  $\Gamma_R$ . When the ball encloses the inclusion, the normal derivative of the solution to the phase conjugation problem (22) coincides with the conjugation of the corresponding recorded data. Thus, we introduce the following first criterion:

$$J_{DN}(B_\rho) := \frac{\left\| \frac{\partial u_R^T}{\partial n} - \frac{\partial \bar{u}^T}{\partial n} \right\|_{L^\infty(\Gamma_R)}}{\left\| \frac{\partial \bar{u}^T}{\partial n} \right\|_{L^\infty(\Gamma_R)}}. \quad (37)$$

The second criterion is derived from the use of absorbing boundary conditions. Indeed, the basis of the method is that the phase conjugated scattered field

$$\bar{u}^S := \bar{u}^T - \bar{u}^I$$

satisfies

$$\text{TRAC}(\bar{u}^S) = \text{TRAC}(\bar{u}^T - \bar{u}^I) = 0 \quad (38)$$

at any point outside the inclusion. In equation (22) this relation is used on the boundary of the artificial ball  $B_\rho$ . Since  $u^T$  is computed numerically and  $u^I$  is given data, that is readily available at any point in  $\Omega \setminus B_\rho$ . Eq. (38) can be computed at any point in  $\Omega$ . Thus, following the principle of the *TRAC* method, we introduce a new boundary  $\Gamma_{J_{ABC}}$  (see Fig. 7) to design a new criterion:

$$J_{ABC}(B_\rho, \Gamma_{J_{ABC}}) := \frac{\|\text{TRAC}(u_R^T - \bar{u}^I)\|_{L^\infty(\Gamma_{J_{ABC}})}}{\|\text{TRAC}(\bar{u}^I)\|_{L^\infty(\Gamma_{J_{ABC}})}}. \quad (39)$$

Note, that this criterion is not based on a direct comparison between numerical data and recorded data in contrast to the first criterion. Hence, it does not require any additional recorded data.

Both criteria (37) and (39) should be zero when the artificial ball  $B_\rho$  encloses the inclusion. Since the *TRAC* is not derived from an exact *ABC*, the above criteria are small but not zero.

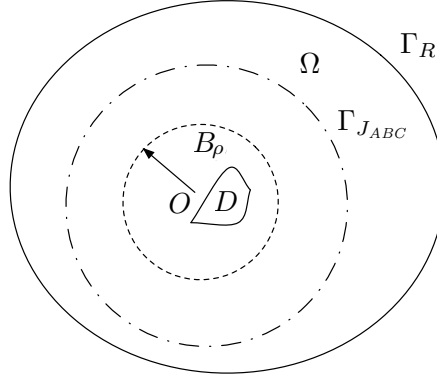


Figure 7: Boundary  $\Gamma_{J_{ABC}}$  inside the region for the new criterion  $J_{ABC}$ .

Since, equation (38) is imposed on  $\partial B_\rho$  in order to compute  $u_R^T$  (see equation (22)), we have to take  $\Gamma_{J_{ABC}}$  different from  $\partial B_\rho$ .

We tested both criteria for a soft circular inclusion of radius two wavelengths ( $2\lambda$ ) with various noise magnitudes on the recorded data defined as in (35). The radius of the artificial ball can be as small as one wavelength and still avoid difficulties because of the absorbing boundary, with a small radius. The results are summarized in Table 3. The results of the enclosing case correspond to a concentric artificial ball  $B_\rho$  of radius  $3\lambda$  and the results of a non enclosing ball correspond to a concentric ball of radius  $\lambda$ . The first criterion  $J_{DN}$  works only up to 5% of noise. However, the use of a filtering technique could improve the domain of validity of this criterion. The second criterion  $J_{ABC}$  enables one to discriminate between the enclosing and non enclosing cases up to 30% noise even though we have not filtered the data. This robustness can be explained by the fact that the noise comes from boundary measurements while, the Helmholtz equation has regularizing properties so that the computed field  $u_R^T$  is much less noisy on the internal boundary  $\Gamma_{J_{ABC}}$  than on the boundary  $\Gamma_R$ .

Noise Magnitude	$J_{DN}$		$J_{ABC}$	
	enclosing	Non enclosing	enclosing	Non enclosing
0%	5.04%	69.20%	6.34%	69.18%
5%	46.38%	93.55%	12.79%	71.62%
10%	103.40%	91.77%	13.55%	70.87%
20%	213.65%	231.30%	35.99%	80.23%
30%	301.46%	269.07%	51.03%	87.80%
40%	532.97%	374.67%	57.99%	84.34%
50%	644.47%	552.57%	63.28%	124.30%

Table 3: Values of the various criteria for several levels of noise.

In the last experiment, we consider a soft inclusion of arbitrary and non smooth shape. We use the *TRAC* method to detect the location of the inclusion by varying the respective locations of the artificial ball. The results are summarized in Table 4. First we take a large ball  $B_\rho$  so that we check that the inclusion  $D$  is not too close to the boundary  $\Gamma_R$ . Then, we move  $B_\rho$  to the left. The high value of the criterion shows us that the inclusion  $D$  is not included inside. The third and fourth show other failed attempts to enclose the inclusion. The last column corresponds to

a successful location of the inclusion. This shows the possibility, by trial and error, to recover the approximate location of the inclusion.

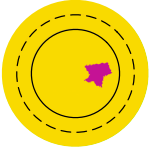

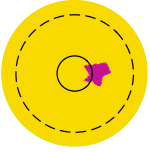
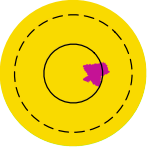
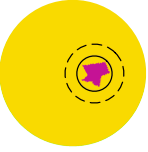
Cases					
$J_{ABC}$	8.52%	66.09%	60.28%	28.35%	11.89%

Table 4: Criterion  $J_{ABC}$  for a soft inclusion and various ball locations.

## 4 Conclusion

We introduce the time-reversed absorbing conditions (*TRAC*) for time-reversal methods. They enable one to “recreate the past” without knowing the source which has emitted the signals that are back-propagated. This is made possible by removing a small region surrounding the source. We present two applications in inverse problems: the reduction of the size of the computational domain and the determination of the location of an unknown inclusion from boundary measurements. We stress that in contrast to many methods in inverse problems, this method does not rely on any *a priori* knowledge of the physical properties of the inclusion. Hard, soft and penetrable inclusions are treated in the same way. The feasibility of the method was shown with both time-dependent and harmonic examples. Moreover, the method has proved to be fairly insensitive with respect to noise in the data.

## References

- [ABB99] Xavier Antoine, Helene Barucq, and A. Bendali. Bayliss-turkel like radiation conditions on surfaces of arbitrary shape. *J. Math. Anal. Appl.*, 229:184–211, 1999.
- [AKNT10] F. Assous, M. Kray, F. Nataf, and E. Turkel. Time reversed absorbing condition. *CR. Acad. Sci. Paris, Ser. I*, 2010. doi:10.1016/j.crma.2010.09.014.
- [BDSG09] Helene Barucq, Rabia Djellouli, and A. Saint-Guirons. Performance assessment of a new class of local absorbing boundary conditions for elliptical- and prolate spheroidal-shaped boundaries. *Appl. Numer. Anal.*, 59:1467–1498, 2009.
- [Ber79] J.R. Berryhill. Wave-equation datuming. *Geophysics*, 44(206):132944, 1979.
- [BF02] Claude Bardos and Mathias Fink. Mathematical foundations of the time reversal mirror. *Asymptot. Anal.*, 29(2):157–182, 2002.
- [BGT82] Alvin Bayliss, Max Gunzburger, and Eli Turkel. Boundary conditions for the numerical solution of elliptic equations in exterior regions. *SIAM J. Appl. Math.*, 42(2):430–451, 1982.
- [BPZ02] P. Blomgren, G. Papanicolaou, and H. Zhao. Super-resolution in time-reversal acoustics. *J. Acoust. Soc. Am.*, 111:230–248, 2002.

- [BT80] A. Bayliss and E. Turkel. Radiation boundary conditions for wave-like equations. *Comm. Pure Appl. Math.*, 33(6):707–725, 1980.
- [CCM00] David Colton, Joe Coyle, and Peter Monk. Recent developments in inverse acoustic scattering theory. *SIAM Rev.*, 42(3):369–414 (electronic), 2000.
- [CK96] David Colton and Andreas Kirsch. A simple method for solving inverse scattering problems in the resonance region. *Inverse Problems*, 12(4):383–393, 1996.
- [CK98] David Colton and Rainer Kress. *Inverse acoustic and electromagnetic scattering theory*, volume 93 of *Applied Mathematical Sciences*. Springer-Verlag, Berlin, second edition, 1998.
- [CM91] J.C. Curlander and R.C. McDonough. *Synthetic Aperture Radar*. Wiley, 1991.
- [dRF02] J. de Rosny and M. Fink. Overcoming the diffraction limit in wave physics using a time-reversal mirror and a novel acoustic sink. *Phys. Rev. Lett.*, 89 (12), 2002.
- [EM77] B. Engquist and A. Majda. Absorbing boundary conditions for the numerical simulation of waves. *Math. Comp.*, 31(139):629–651, 1977.
- [Fin09] M. Fink. *Renversement du temps, ondes et innovation*. Ed. Fayard, 2009.
- [FWCM91] M. Fink, F. Wu, D. Cassereau, and R. Mallart. Imaging through inhomogeneous media using time reversal mirrors. *Ultrasonic Imaging*, 13(2):199 – 199, 1991.
- [Hec10] Frédéric Hecht. *FreeFem++*. Numerical Mathematics and Scientific Computation. Laboratoire J.L. Lions, Université Pierre et Marie Curie, <http://www.freefem.org/ff++/>, 3.7 edition, 2010.
- [KTU87] Gregory Kriegsmann, Allen Taflove, and K.R. Umashankar. A new formulation of electromagnetic scattering using on surface radiation condition approach. *IEEE Trans. Ant. Prop.*, AP35:153–161, 1987.
- [LD03] Sean K. Lehman and Anthony J. Devaney. Transmission mode time-reversal super-resolution imaging. *J. Acoust. Soc. Am.*, 113 2742, 2003.
- [LMF<sup>+</sup>06] C. Larmat, J.-P. Montagner, M. Fink, Y. Capdeville, A. Tourin, and E. Clévéde. Time-reversal imaging of seismic sources and application to the great sumatra earthquake. *Geophys. Res. Lett.*, 33, 2006.
- [MT09] Michael Medvinsky and Eli Turkel. On surface radiation conditions for an ellipse. *JCAM*, 234:1647–1655, 2009.
- [MTH08] Michael Medvinsky, Eli Turkel, and Ulrich Hetmaniuk. Local absorbing boundary conditions for elliptical shaped boundaries. *J. Comput. Phys.*, 227(18):8254–8267, 2008.
- [PMSF96] C. Prada, S. Manneville, D. Spoliansky, and M. Fink. Decomposition of the time reversal operator: Application to detection and selective focusing on two scatterers. *J. Acoust. Soc. Am.*, 99 (4):2067–2076, 1996.
- [STX<sup>+</sup>05] R. Sinkus, M. Tanter, T. Xydeas, S. Catheline, J. Bercoff, and M. Fink. Viscoelastic shear properties of in vivo breast lesions measured by mr elastography. 23(2):159–165, 2005.

- [The92] C. W. Therrien. *Discrete Random Signals and Statistical Signal Processing*. Englewood Cliffs, NJ: Prentice- Hall, 1992.